Multiple DD fusion events at interelectrode media of nanosecond vacuum discharge

2006 J. Phys. A: Math. Gen. 39 4375

(http://iopscience.iop.org/0305-4470/39/17/S11)

INSTITUTE OF PHYSICS PUBLISHING JOURNAL OF PHYSICS A: MATHEMATICAL AND GENERAL

J. Phys. A: Math. Gen. **39** (2006) 4375–4386 doi:10.1088/0305-4470/39/17/S11

Multiple DD fusion events at interelectrode media of nanosecond vacuum discharge

Yu K Kurilenkov[1], **M Skowronek**[2] **and J Dufty**[3]

[1] Institute for High Temperatures of Russian Academy of Sciences, 13/19 Izhorskaya Str., 125412 Moscow, Russia
[2] Laboratoire des Plasmas Denses, Université Pierre et Marie Curie, F-75252 Paris Cedex 05, France
[3] Department of Physics, University of Florida, Gainsville, FL 32611, USA

E-mail: ykur@online.ru, maurice.skowronek@noos.fr and dufty@phys.ufl.edu

Received 4 October 2005, in final form 5 January 2006
Published 7 April 2006
Online at stacks.iop.org/JPhysA/39/4375

Abstract

We create and operate with a random interelectrode media of high power density using the low energy nanosecond vacuum discharges. The subjects of our study are hard x-ray emission efficiency, generation of energetic ions ($\sim$1 MeV) and neutrons and the trapping and release of fast ions and/or x-rays from interelectrode complex ensembles of cold micro grains with some micro plasmas. The value of the neutron yield from DD microfusion in the interelectrode space is variable and amounts to $\sim 10^5$–$10^7/4\pi$ per shot under $\approx$1 J of total energy stored to create all discharge processes. In a limiting case of total trapping of fast deuterium ions by the dense 'dusty cloud' of clusters under partial hard x-ray diffusion and multiple fusion events inside, the pulsating neutron yield has maximum values (table-top complex plasma 'microreactor'). The role of virtual cathode formation and electrostatic mechanism of ions acceleration at the regime of unstable current carrying are discussed briefly.

PACS numbers: 52.40.Mj, 52.57.Lw, 52.58.Qv, 52.59.Px, 52.80.Vp

1. Introduction

Rather simple small-scale experiments carried out during the last decade provide much information that is complimentary to available large-scale studies of high energy density matter physics. For example, table-top experiments using femtosecond laser irradiation of clouds of clusters [1] have demonstrated how x-rays, fast ions and even neutrons can be generated. Different states of matter in unusual conditions and many intriguing physical problems have been realized also by the study of vacuum discharges, where an extensive

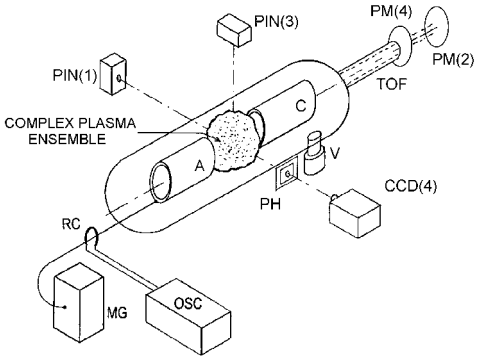

Figure 1. Schematic of the experiment for generating interelectrode complex plasma ensembles with multiple DD fusion events: MG, Marx generator; RC, Rogovskii coil; A and C, anode and cathode; PIN, instant PIN diodes; CCD, camera; PH, pinhole; PM2 and PM4, photomultipliers; OSC, oscilloscope; TOF, time of flight tube; V, vacuum pump.

experience has been accumulated [2, 3]. Indeed, vacuum discharges alone, even without laser irradiation, can be used to create foam-like 'targets' in high power density matter studies.

Earlier, different possibilities of x-ray and neutron generation under reasonable vacuum spark discharge conditions have been demonstrated and studied by a number of authors (see, for example, [4–10] and references therein). The most detailed knowledge has been obtained in studies of magnetically compressed (pinched) regions of microplasmas under extreme conditions (mainly, under ∼kJ and $\sim 10^2$ kA machines), although the possible role of dusty particles for energy concentration in 'hot spots' has also been discussed (cf [10]). It would therefore be of interest to try to operate vacuum spark discharge with stochastic media in a more systematic manner and under more moderate discharge conditions (∼1 J, ∼1 kA). The present work concerns an attempt to incorporate some collective, coupling and anomalous effects simultaneously in order to produce high power density foam-like interelectrode working media for DD nuclear reactions using a hollow cathode low energy vacuum discharge [11, 12].

Complex plasma ensembles of high power density (cold clusters with a possible small fraction of hot microplasmas) are generated by an intense energy deposition into the cold solid density but low volume dusty 'target' collected especially in the interelectrode space (clusters, nanoparticles of different size condensed from the vapours of anode material). This foam-like erosion 'target' forms automatically behind the anode flare during the pre-breakdown stage at the chosen discharge conditions after a high voltage is applied (see [11, 12] for the details of the experimental set-up presented in figure 1). The current-carrying stage is accompanied by intense emission of hard x-rays from interelectrode complex plasma ensembles. Simultaneously with hard x-rays, the generation of hot electrons and energetic ions with energies about 0.1–1 MeV or higher also occurs (the energy is estimated from time of flight (TOF) measurements with Fe anode [11]). Both electrons and ions ultimately have to reach the speed of sound in the hydrodynamically expanding microplasmas or be accelerated by specific plasma collective fields appearing sometimes in the interelectrode space [13]. Most of the kinetic energies are contained in the ions since their mass is much greater. As a result, in spite of still poorly clarified mechanism of ions acceleration, the interior of the interelectrode ensembles (or some local areas) may resemble something like a microreactor due to *head-on collisions of fast ions and/or their stopping* on the cold cluster target. This should allow us to study the nuclear synthesis microevents (e.g. DD microfusion) [12] and to investigate

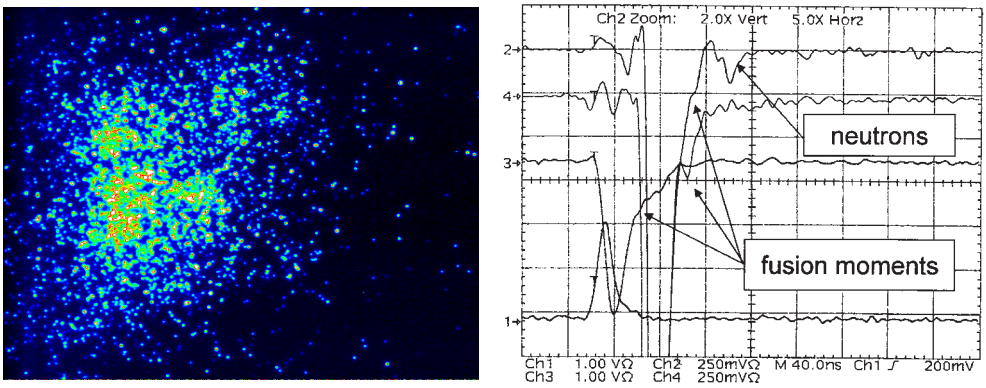

(*a*) (*b*)

Figure 2. (*a*) Hard x-ray CCD image of low density and transparent interelectrode ensemble with DD reactions accompanied by moderate neutron yield ($\sim 10^6/4\pi$, assuming isotropic yield). (*b*) The extra hard x-rays at channel 4 indicate the beginning of nuclear reactions (sensitivity of channel 2 is 250 mV; grid step is 40 ns). The delay of the neutron peak at channel 2 corresponds to $\approx$46.6 ns m^{-1} (2.45 MeV neutrons due to DD burning).

the neutron yield as a function of ensemble density, geometry and other experimental conditions.

2. Experimental set-up: DD microfusion and neutron yield

The plasma source (figure 1) [11, 12] consists of a cylindrical vacuum chamber (diameter 50 mm) having three windows closed by Mylar films 70 μm thick. This cylinder is connected to a vacuum pump able to reach 10^{-6} to 10^{-7} mbar and working in a continuous regime throughout the series of discharge shots. Two electrodes are included on the cylinder axis: a hollow anode and a hollow cathode having different shapes. The distance between the electrodes can vary by 0.1 mm steps up to 6–7 mm maximum. The source is included in a coaxial high voltage cable having 50 Ω impedance, which is connected to a four-stage Marx generator ($\approx$1 J) delivering a 50 ns pulse of maximum voltage 70 kV in a 50 Ω load. The value of the current is usually 1 kA. Three Mylar windows allow the x-ray intensity measurement in three perpendicular directions (side-on right, left and upper ones) in the plane corresponding to the anode edge. Another Mylar window and/or TOF tube allows the end-on measurement through the hollow cathode. Calibrated PIN diodes having a 1 to 2 ns rise time are used to measure the x-ray output. The x-ray CCD image of sources is obtained by means of a pinhole with diameter less than 0.1 mm bored in a 1 mm thick lead screen covered by a 100 μm thick Al foil.

Neutron generation in x-ray ensembles (like in figures 2(*a*) and 3(*a*)) due to DD reactions of nuclear synthesis has been registered using a slightly modified experimental set-up in comparison with earlier x-ray and fast ions studies [11]. Also, we have used a particular modified and deuterated Cu–Pd anode. (The standard electrolysis in heavy water for about 6 h at a current of 100 mA has been used for partial saturation of Pd elements of the anode by deuterium). Note that channels 1 and 3 (figure 1) represent the x-ray intensity from instant PIN diodes which have a maximum sensitivity at $\approx$10 keV. Harder x-rays (with energy $>$60 keV) are registered by PM2 covered usually by a 2 mm Cu absorber (the signal at channel 2 is delayed due to electronic scheme of PM2 for $\approx$35 ns in comparison with the instant

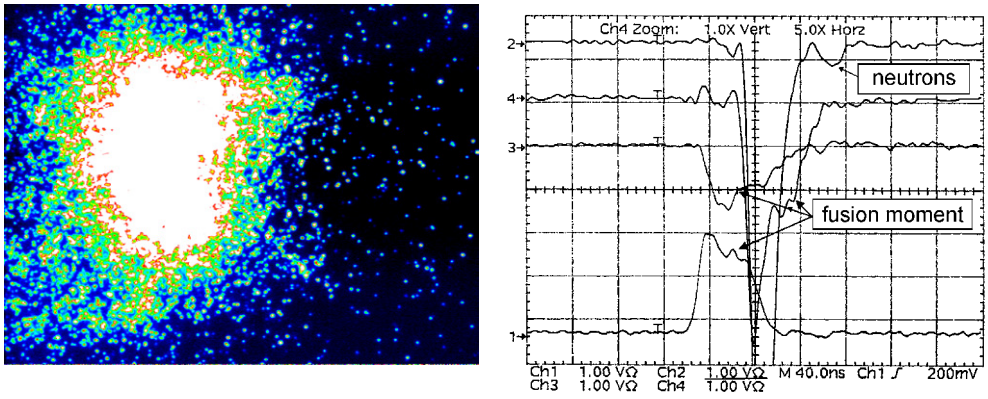

(*a*) (*b*)

Figure 3. (*a*) Dense complex plasma ensemble with DD microfusion events and higher neutron yield ($\sim 10^7/4\pi$). (*b*) Stronger and broader neutron peak than in figure 2(*b*) (sensitivity of channel 2 is lower than in figure 2(*b*), 1V). This reference moment of DD burning is represented also by changing of PIN's signals.

PIN diodes signals for all oscillograms presented below). TOF measurements have been performed with photomultipliers PM4 and PM2 (figure 1), located along the electrode axes at the distances of 45 cm and 50–90 cm, correspondingly (channels 4 and 2 on oscillograms like figures 2(*b*) and 3(*b*); photomultipliers were screened and covered by scintillators which were designed in a different manner to register neutrons if available, PM2, or register extra x-rays due to the moment of DD reaction itself, PM4). Beyond the usual hard x-rays (first strong peak at channel 2), PM2 may indicate the well-reproducible signal (second small peak) with a delay of about 46.6 ns m^{-1}, typical for 2.45 MeV neutrons from DD synthesis reactions. Meanwhile, PM4 which is located usually between the source and PM2 has to register especially the moment of time when fusion events may take place (if the main x-ray peak itself will not be too broad to avoid the screening of this natural 'reference point' as illustrated in figures 2(*b*) and 3(*b*)). The second small peak from PM2 (distance $L = 90$ cm) corresponds to the neutron yield due to D + D = n + He^3 reaction (like in figures 2(*b*) and 3(*b*)). The changing of the distances between dusty hard x-ray source and PM2 is followed by the corresponding displacement of the second (neutron) peak. The plates CR39 and PN3 have been used simultaneously with the TOF scheme to detect neutrons. Their development shows the variable number of tracks which has to be attributed to neutrons also. The minimal energy of deuterons, E_D, estimated from the spread of arrival times $\Delta t \approx 778\, d_{SD}(E_D)^{1/2}$ of neutrons at a detector is about 20 keV (d_{SD} is the distance from source to detector in metres, E_D is ion energy in keV) [14].

The magnitudes of the particular TOF's peaks measured by PMs, numbers of tracks related to PN3 (CR-39) plates, hard x-ray CCD images registered are in good and reproducible correlation (brightness of CCD images presented in colour is proportional to hard x-rays intensity registered). The number of tracks increases with the number of shots also. The value of the neutron yield from random interelectrode 'dusty' media is variable, and turns out to be about 10^5–$10^7/4\pi$ per shot under $\approx$1 J of *total* energy deposited to create all the discharge processes at the single shot (assuming isotropic yield). In fact, a typical example from the x-rays database of images of interelectrodes dusty matter with lower neutron yield (and low total x-ray ones) is shown in figure 2(*a*). Namely, rather low x-ray yield allows us to register more accurately the moment of microfusion events. The ensembles with more

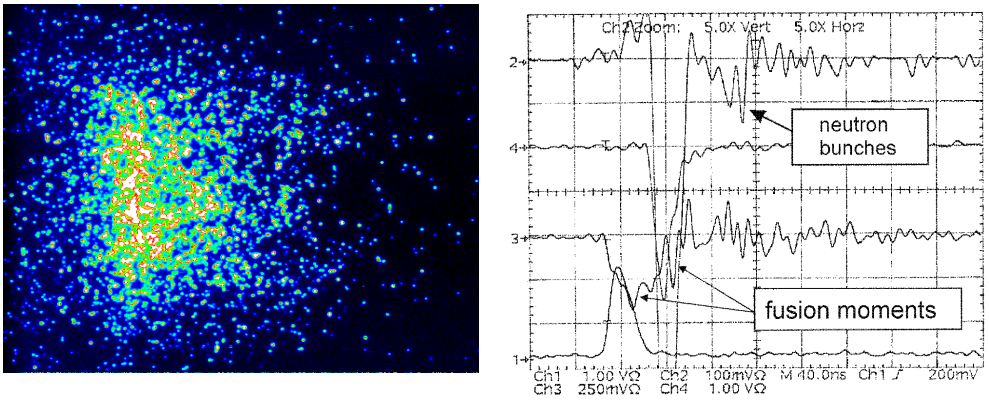

(*a*) (*b*)

Figure 4. (*a*) CCD camera image of hard x-rays from dilute and transparent cluster ensemble with *multiple DD fusion* events. (*b*) Nanosecond-scale growing bunches of neutrons, channel 2. A few extra x-ray spikes on channel 3 indicate the consequent moments of DD reactions.

saturated x-ray images correspond to higher neutron yields (figure 3(*b*); the sensitivities of channel 2 in figures 2 and 3 are different). Linearity of the function 'neutron yield–total x-ray intensity' applies to the range indicated above for the neutron yield, and this tendency is illustrated qualitatively by the images and neutron peak intensities for the typical certain class of cluster ensembles as presented in figures 2 and 3. At this range, the hard x-rays may release from the ensembles, while fast ions have to be partially 'stopped' at different levels by cluster clouds of variable density [12].

3. Trapped fast ions, diffused x-rays and multiple fusion events

Another possible feature of neutron yield is illustrated by the shot presented in figures 4(*a*) and (*b*). The CCD image in figure 4(*a*) shows the ensemble of an intermediate density of clusters, but the oscillograms (channel 2, PM2, $L = 55$ cm, sensitivity of 100 mV) manifest an essential *pulsating neutron yield* (figure 4(*b*)), which is increasing from bunch to bunch of neutrons. These *multiple fusion events* (MFE) at 'dusty' ensembles could be due to the development of some current-carrying collective instability or under different percolation paths of current passing through an ensemble of microparticles of strongly heterogeneous sizes. Correspondent extra x-rays due to each DD fusion event are registered as fractures both at the PIN diode (channel 3) and at the PM4 signals of hard x-rays intensity (the right parts of these x-ray intensity curves are modulated by the same moments of fusion with a delay of $\approx$35 ns in comparison with instant diodes signals, channels 1 and 3). The intensity of the last neutron peaks registered is weakened partially due to a possible reflection from the 2 mm Pb absorber located in front of PM2. Note that elements of minimum two fusion events (channels 1, 2 and 3) followed by two merged neutron peaks (channel 2) might be recognized also in oscillograms of figure 3(*b*).

Another effect may appear if the concentration of grains is increased but their mean sizes decreased (we have $\approx$0.01–1 μm in comparison with $\sim 10^{-3}$ μm at laser focusing on clusters [1]). By varying the interelectrode volume within an order of magnitude (by changing A–C distance, 0.5–0.1 cm) under approximately the same value of mass transfer from anode ($\sim 10^{-7}$ g) and under smooth variation of the pressure at the range 10^{-6}–10^{-2} mbar (which

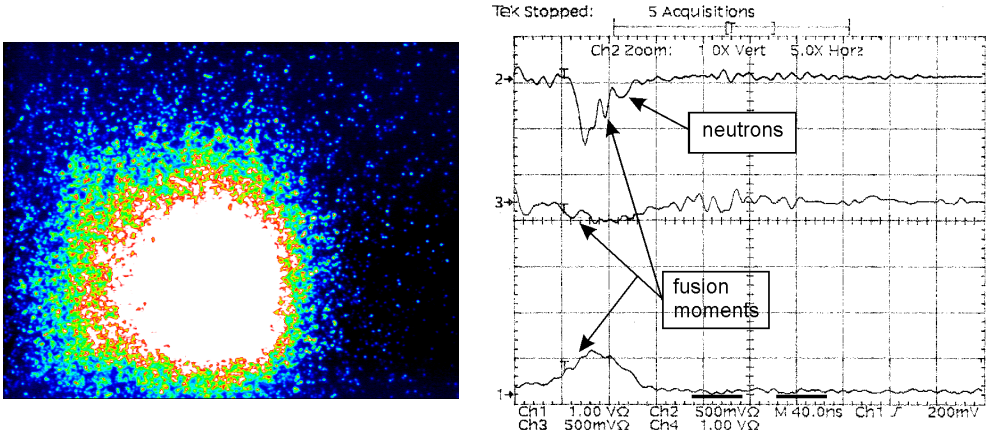

(*a*) (*b*)

Figure 5. (*a*) CCD camera image of hard x-rays from dense partially self-organized cluster ensemble as neutron source (x-rays 'ball', $\varnothing \approx 0.5$ cm, or nanoparticle 'microreactor'). (*b*) X-rays generated are diffused partially inside the 'ball' and are released rather slowly, mainly from the skin-layer (channels 1 and 3). Total fast ion trapping at TOF regime (channel 2).

influences essentially the processes of nucleation), we may regulate partially the level of x-ray absorption and multiple scattering inside the ensemble of clusters. In general, being trapped in a disordered system in the diffuse regime, $\lambda \ll l_{sc} \ll R$, light may make a long random walk before it leaves the medium from the nearby surface area [15–17] ($l_{sc} = 1/N_0 Q_S$, mean free path of photons due to scattering; R, ensemble dimension; λ, the wavelength; Q_S, scattering cross section; N_0, volume density of scattering particles; $N_0^{-1/3} \gg \lambda$). In fact, the dynamics of x-ray radiation at the regime close to x-ray diffusion (figure 5) has interesting properties, differing from ordinary (transparent or disordered) x-ray ensembles as in figures 2–4. In real time the diffused lower energy x-ray photons (energy ~3–10 keV) are delayed to appear from a *self-organized 'ball'* interior in comparison with very hard x-ray emission (channel 2, photon energy $\geqslant$60 keV) which is not trapped. Since PIN diode signals in the diffuse regime (figures 5(*a*) and (*b*)) are suppressed in intensity due to absorption but extended in time, we do not observe the standard electronic delay of photomultiplier signals (~35 ns) in comparison with the PIN diode ones as is usual for the non-diffuse regimes (like in figures 2(*b*)–4(*b*)). The distance 'x-ray source–PM2' for the shot in figure 5 was about 50 cm and PM4 was removed at this short distance, but the fusion moment is registered noticeably by the PIN diodes and mainly by PM2 itself as well (figure 5(*b*)). (Extra hard x-rays small peak due to microfusion at channel 3 is not behind the main x-rays peak in time as usual, figures 2 and 3, but in front of diffused x-rays released from ensemble, figure 5). Meanwhile, fast ions are completely trapped for this type of ensemble (no TOF ion signal at PM2, channel 2 sensitivity is 500 mV).

It appears reasonable to try to combine the advantages of interelectrode cluster ensembles with multiple fusion events (figure 4) and with *diffused x-rays under total trapping of fast ions* (figure 5). Namely, one of the cluster ensembles with similar combined features is shown in figure 6 as the prototype of a table-top *complex plasma microreactor.* We observe a bright image of a quasi symmetrical cluster ensemble, but with very low hard x-ray yield under their partial diffusion (channels 1 and 3). The growing (left) part of intensity curve from PM4 (channel 4) represents mainly the extra x-rays due to fusion events with few corresponding peaks. The main part of intensity registered by PM2 (channel 2) represents the strong pulsating

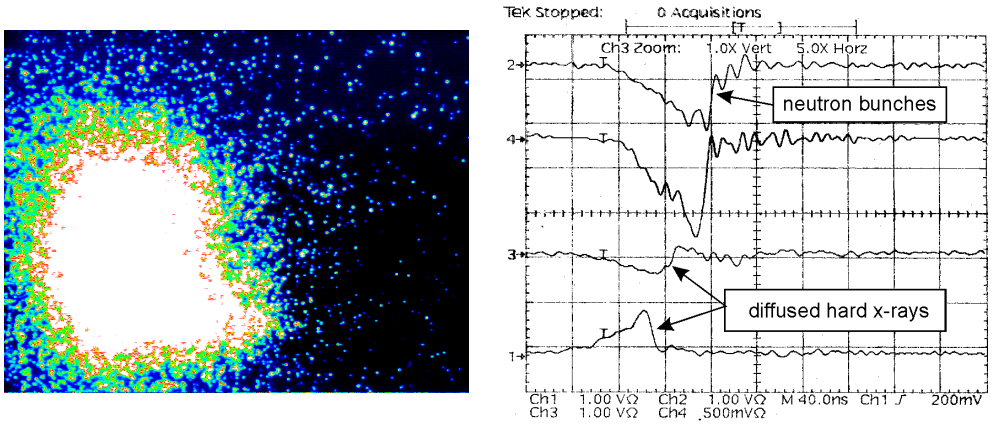

(*a*) (*b*)

Figure 6. (*a*) CCD image of dense quasi-symmetrical cluster ensemble with *trapped fast ions and multiple DD fusion events* (complex plasma 'microreactor'). (*b*) Diffused hard x-ray escapes with partial delay (channels 1 and 3, as in figure 5), and a few peaks of extra x-rays at fusion moments (channel 4, left part of curve) are followed by enhanced pulsating neutron yield (channel 2, main oscillating part of curve).

neutron yield as a manifestation of 'waves' of DD microfusion from a nanoparticle ensemble ($L = 90$ cm, 0.5 mm Cu absorber, channel 2 sensitivity is 1 V). The sensitivity of channel 4 ($L = 45$ cm, 500 mV; 0.5 mm Cu) is higher than that for channel 2 in contrast to the previous data in figures 3, 4 and 5. This means that mainly the process of neutrons coming was registered by PM2. Note that the bright ensembles of figures 5(*a*) and 6(*a*) at photon diffusion give lower but longer low x-ray emission intensities, while the partial trapping of photons and total trapping of fast ions do increase neutron yield due to MFE at least a few times (under the same level of deuteration of Pd anode). Underline, the shot presented in figure 6 has been performed under very similar conditions as the previous one (figure 3); however, some self-organization of cluster ensemble (like in figure 5) was followed by noticeable decreasing of total x-rays release in comparison with shot in figure 3. (Concerning x-rays 'trapping', the shot in figure 6 represents an intermediate case between ones presented in figures 3 and 5.)

We remark that usually the set of oscillograms for each shot represents essential and complete information about complex ensembles and specific processes. However, the first or immediate interpretation of the oscillograms for systems with MFE and diffused x-rays (like in figure 6) is not so evident a task, and has to rely upon the entire available database for radiation from interelectrode cluster media and CCD images. To illustrate some of the internal processes we may take one step back. Below we present an example of particular ensemble (figure 7) with a lower density of clusters and partially destroyed symmetry, but also with MFE and under partially diffused x-rays. To suppress own hard x-rays from cluster ensemble which are mixed with neutron signals (like at channel 2, figure 6) and with extra x-rays at fusion moments (channel 4, figure 6) we are using a Pb screen (3 mm thick) in front of PM2 (channel 2). A sharp and strong peak at channel 2 (figure 7) corresponds to very hard x-rays at the front of pulse, and less hard x-rays at later times are absorbed. A small intensity peak almost immediately after the maximum indicates extra x-rays from first fusion moment (channel 2, figure 7). This moment coincides also with the first small peak at channel 4 as well as with beginning of variation of the PIN diode signal in real time (channel 3, at about 35 ns left at time scale). Thus, general x-rays from the ensemble, channel 4, are modulated by extra

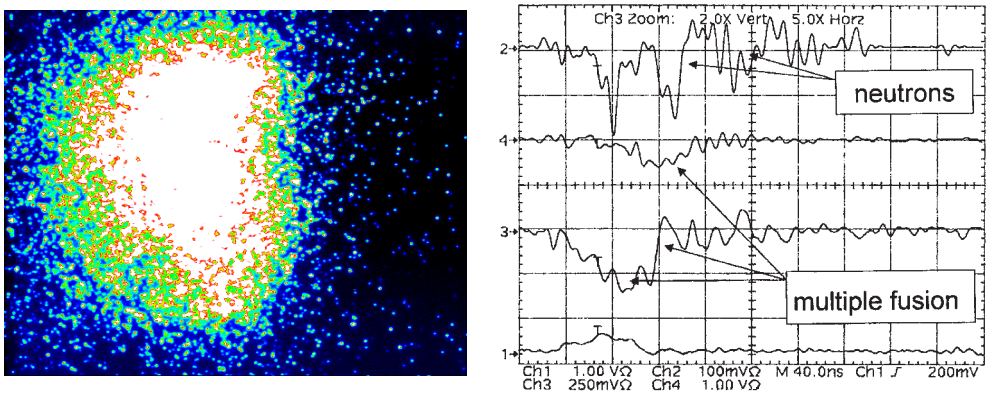

(*a*) (*b*)

Figure 7. (*a*) CCD camera image of hard x-rays from typical cluster ensemble of intermediate density with multiple DD fusion. (*b*) Oscillograms indicate a few consequent moments of DD burning (correlated signals at channels 3 and 4). Own harder x-rays are strongly absorbed by Pb screen (channel 2).

x-rays from multiple DD fusion events (this effect of signal modulation is clearly represented in whole by the x-ray intensity curve from channel 3 also). Correspondingly, the set of neutron bunches with intermittent intensities is registered by PM2 (channel 2, a few neutron signals are weakened because of their partial reflection from Pb slit; remark that reflections from Pb may sometimes create induced noise signals at PM2,4 also). This is a typical ensemble with MFE, when consequent fusion moments have been registered by channels 1, 3 and 4 (figure 7). A similar structure of oscillograms (like figure 7(*b*)) is easily reproducing from shot to shot for different random configurations of interelectrode cluster ensembles and represents an essential part of database accumulated at the present stage of the work; meanwhile, ensembles like in figure 6 are more rare. On the whole, typical hierarchy of related times at MFE for particular fusion moment contains usually the instant signal from channel 1 or channel 3 at the moment t_f, next, electronically delayed signal at channel 4, t_f + 35 ns and time of flight delayed neutron signal at channel 2, t_f + 35 ns + t_{TOF}, correspondingly.

Thus, the set of the results obtained shows that the simple nanosecond-scale discharge scheme suggested here to produce x-rays and neutrons from approximately 1 J of energy in the discharge is complementary to advanced and instructive table-top schemes such as laser-irradiated clusters [1]. The efficiency of neutron production at our low-energy discharge (as well as hard x-rays) may be two orders of magnitude higher than for fusion events driven by laser-irradiated clusters explosions (10^4 neutrons for 120 mJ of *laser* energy [2]), while the total estimated number of deuterons in the laser focal area [2] and ejected from anode into interelectrode space at our single shot is of the same order ($\sim 10^{13}$–10^{14}). This efficiency has been realized due to several reasons [12] and, in particular, due to the fact that for experiments [1] with fusion driven by Coulomb explosion of clusters the collisional free path l_D for ions D^+ is much longer than the plasma dimension (which is about laser focal diameter d_{focal} = 200 μm), $l_D \gg d_{focal}$. In our case, the smooth variation of the relation between l_D and cluster ensemble radius, R_{ball}, is possible. As a result, it may include even the trapping of all the deuterium fast ions (figure 5) generated inside the ensemble of cold grains, $l_D < R_{ball}$ (‘*dusty*’ *stopping*). Thus, it is rather natural that the neutron yields in fact will be higher for ensembles with brighter CCD camera images of systems, which have a lower transparency for x-rays and

fast ions. Meanwhile, new qualities of interelectrode cluster ensembles such as experimentally recognized MFE and x-rays diffusion inside represent another potential opportunity for further optimization of neutron yield.

4. Remarks on collective ions acceleration

The ensembles in interelectrode space in vacuum discharges are analogous in some respects to foam-like laser target systems suggested earlier for efficient neutron generation [18]. However, the mechanisms themselves of ion accelerations may be essentially different. In particular, besides possible Joule anomalous overheating of particular clusters by carrying current, other mechanisms of ion acceleration by collective fields (∼eZ) of a different nature and time-space scales might be realized for the complex interelectrode plasma and need correspondent analysis [12, 13, 19]. Earlier, the relationship was established experimentally [19] between current instabilities of vacuum spark and the appearance of anomalously accelerated ions (ion energies reached 10–15 MeV under just 300 kV applied to the gap). In the stable regime [19] current extraction followed to the low $3/2$ while in the unstable regime the emission current exceeds Langmuir limit [2,10], which is manifest as an abrupt short-lived ∼5 ns burst. An emission current burst was accompanied by an increase of the potential of plasma layers near the front of the cathode jet. An electrostatic model based on the concept of a deep potential well for a virtual cathode was developed recently [13], in particular, to explain the anomalous ion acceleration and current bursts observed in experiments [19, 20]. It was shown that the process of formation and destruction of the potential well may be repeated and results in multiple bursts of anode current and pulse fluxes of accelerated ions and electrons. Effective acceleration can be achieved if the lifetime of the well T_W is more than oscillation period $\left(\sim\omega_{pi}^{-1}\right)$ of the ions trapped in the well. The half-width of the nonstationary potential well was estimated as $l_W \approx 2v_0/\omega_{pe}$, where v_0 is the electron velocity. A value of $l_W \approx 0.3$ cm was obtained from experiment [19] with interelectrode gap length $d = 2$ cm.

The main features recognized for collective ions acceleration at the systems with electron beam injection into drift space and virtual cathodes have to be incorporated for further analysis of our scheme of vacuum discharge (cf [21–23] and review [24, first part] as well as comments related [24, second part]). 'Dusty'-like anode plasmas (virtual anode) with immersed virtual cathode deep inside have to represent the essential specifics of the complex plasma 'microreactor' considered [12]. Formation of a virtual cathode and corresponding potential wells would be provided by cylindrical symmetry of the electrodes in our discharge. Trembling of the virtual cathode as well as unstable regime of current carrying near Langmuir limit would result in ion acceleration accompanied by pulsating neutron yield (like in figures 4, 6 and 7). Simulation of virtual electrodes and potential wells dynamics for our discharge geometry with fully electrodynamic code [25] is the subject of present work [26] to understand better the complicated and contradictory nature of ions acceleration [24].

Meanwhile, applying an electrostatic model in analogy to [13, 19], for conditions of our experiment the value of potential well half-width could be estimated as $l_W \approx 0.05$–0.1 cm ($d \approx 0.2$–0.5 cm under non-planar electrode geometry). We remark that the duration of short-lived burst (or duration of ions acceleration) [19] is approximately equal to the fusion moment duration (extra x-ray peaks like in figure 2, channel 4). In other words, probably the extra x-ray half-width is an estimation or indirect measure of the lifetime of potential well deformation as well as ions acceleration time in our case. The electrostatic mechanism of ion acceleration in our experiment is confirmed partially by their energy distribution, represented qualitatively by histograms for ion track size from CR39 plates used separately. (Track size is approximately proportional to ion energy.)

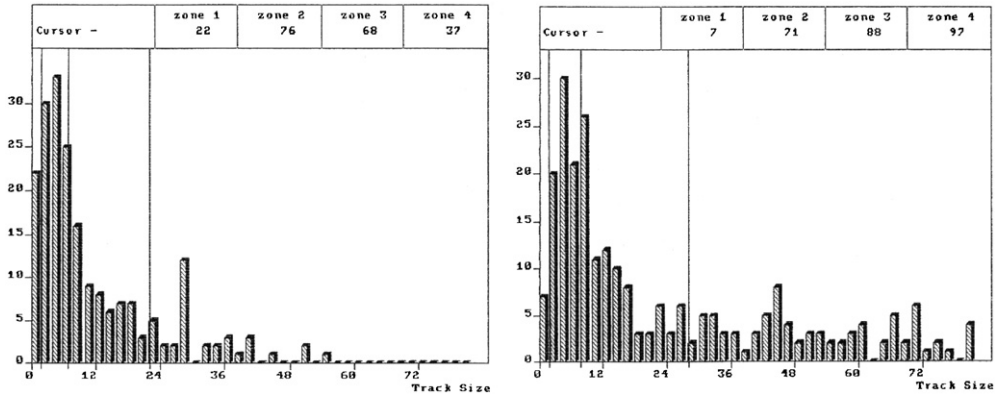

Figure 8. Histogram for energy distribution of fast ions from CR-39 plates (number of tracks versus track size): (*a*) standard Fe anode; (*b*) Cu–Pd anode for DD reactions yield study (see text).

Figure 8(*a*) shows the distribution for a standard Fe anode used at the beginning, and figure 8(*b*) represents the traces for Cu–Pd anode designed and used in our DD fusion experiments. The long 'tail' as *plateau* for the fast ion energy distribution (figure 8(*b*)) has an energy cut-off of about ≈3 MeV as the minimum. The maximum number of tracks on the histogram in figure 8(*a*) corresponds to typical energies obtained from TOF measurements for fast ions (≈300 keV) [11, 12]. Thus, the Gamov peak for the yield of the DD reaction was enhanced under our experimental conditions due to the electrostatically accelerated D^+ in the energy interval as minimum ≈10–50 keV.

It would be instructive to analyse some similarities on long-time activity in inertial electrostatic confinement fusion (IECF) and of nanosecond small-scale vacuum discharge scheme presented (for background, keys issues and IECF attractiveness, see [27, 28] and references therein). In particular, note that single, double and multiple well formations, non-Maxwellian ion energy distributions and non-ignited plasma are also typical phenomena for IECF. We emphasize that the study of correlation between potential well structure and neutron production in IECF has recognized that not only the potential well depth itself but namely the unstable behaviour of the potential may provide high neutron production under beam–beam interactions [28]. Qualitatively, a similar effect from our study is represented in the typical figure 7(*b*) scope traces with MFE under possible virtual electrode formation in vacuum discharge. Total neutron yield per second at IECF stationary regimes may be comparable with neutron yield from our discharge during ∼50 ns (order of $\sim 10^6$–10^8 in isotropy approximation). We remark that as is typically for IECF, our scheme is also very far from 'break-even' ($Q \sim 10^{-6}$). From the other side, partial or essential trapping of x-rays and fast ions recognized for interelectrode ensembles (like in figures 5 and 6) demonstrates the general ability for *energy capture* at a 'dusty' microreactor. Moreover, some rare shots manifest also the possibility of essential self-organization of cluster ensembles followed by extremely low x-ray yields [29]. Meanwhile, if the energy gains under photon diffusion through the volume would exceed surface losses, strong x-ray bursts with typical spikes [11, 29] may occur reminiscent of random lasing [15–17]. These last two features of interelectrode clusters ensembles are subject of further study also.

In summary, during the last decade various small-scale experiments have demonstrated the opportunity to accelerate deuterium ions towards a solid target or another ion with 2.45 MeV neutron yields registered as the signature of DD nuclear reactions (see, for example,

[1, 30] and the references therein). Also, low energy but pulsed power discharge with specific virtual cathode to accelerate ions at the regime near limiting current represents a rather simple tool to study collisional DD fusion physics as well as perhaps for nuclear science education. Practically, as presented and discussed above, the miniature complex interelectrode plasma ensembles with multiple fusion events under low energy applied, in particular, allow pulsed measurements if developed. Safety procedures for deployment and storage could be simplified, for example, in comparison with radioisotope neutron sources because the dusty 'microreactor' can be simply turned off. Also, nanosecond-scale neutron bursts might provide the time-of-flight scheme to determine the distance to a target for detecting materials.

Acknowledgments

We would like to thank G A Mesyats, A A Rukhadze, G Maynard and Y Vitel for interest and support of the work as well as for critical remarks and stimulating discussions. We acknowledge partial support of this work by the Program for Fundamental Research of Russian Academy of Sciences and NATO Science Program grant PST. NR. CLG. 980685.

References

[1] Ditmire T, Zweiback J, Yanovsky V P, Cowan T E, Hays G and Warton K B 1999 *Nature* **398** 489
Zweiback J *et al* 2000 *Phys. Rev. Lett.* **84** 634
[2] Mesyats G A and Proskurovsky D I 1989 *Pulsed Electrical Discharge in Vacuum* (Berlin: Springer)
[3] Boxman R L, Goldman S and Greenwood A 1997 *IEEE Trans. Plasma Sci.* **25** 1174–86
[4] Cohen L, Feldman U, Swartz M and Underwood J H 1968 *J. Opt. Soc. Am.* **58** 843
[5] Schwob J L and Frenkel B S 1972 *Phys. Lett.* A **40** 81
[6] Lie T and Elton R C 1971 *Phys. Rev.* A **3** 865
[7] Feldman U, Goldsmith S, Schwob J L and Doschek A 1975 *Astrophys. J.* **201** 225
[8] Negus C R and Peacock N J 1979 *J. Phys. D: Appl. Phys.* **12** 91
[9] Lee S and Conrads H 1976 *Phys. Lett.* A **57** 233
[10] Mesyats G A 2000 *Cathode Phenomena in a Vacuum Discharge: The Breakdown, the Spark, and the Arc* (Moscow: Nauka)
[11] Kurilenkov Yu K, Skowronek M, Louvet G, Rukhadze A A and Dufty J 2000 *J. Phys.* **10** Pr5–409 IV
[12] Kurilenkov Yu K and Skowronek M 2003 *Pramana J. Phys.* **61** 1188–96 (Indian Academy of Sciences)
Kurilenkov Yu K and Skowronek M 2005 *Proc. 15th Int. Conf. on MHD Energy Conversion and VI Workshop on Magnetoplasma Aerodynamics for Aerospace Applications (Moscow, 24–27 May)* pp 206–17
[13] Barengol'ts S A, Mesyats G A and Perel'shtein E A 2000 *JETP* **91** 1176
[14] Lerche R A, Phillion D W and Tietbohl G L 1995 *Rev. Sci. Instrum.* **66** 933
[15] Letokhov V S 1968 *Sov. Phys.—JETP* **26** 835–40
[16] Wiersma D and Lagendijk A 1996 *Phys. Rev.* E **54** 4256–65
Wiersma D and Lagendijk A 1997 *Phys. World* **10** 33–7
[17] van Albada M P, van Tiggen B A, Lagendijk Ad and Tip A 1991 *Phys. Rev. Lett.* **66** 3132
[18] Gus'kov S Y, Zmitrenko N V and Rozanov V B 1999 *Lett. JETP* **66** 521
[19] Plyutto A A 1960 *JETP* **12** 1106
Korop E D and Plyutto A A 1970 *J. Tech. Phys.* **40** 2534 (Russian)
Korop E D and Plyutto A A 1970 *Sov. Phys. Tech. Phys.* **15** 1986
[20] Proskurovskii D I *et al* 1975 *J. Tech. Phys.* **45** 2135 (Russian)
Proskurovskii D I *et al* 1975 *Sov. Phys. Tech. Phys* **20** 1342
[21] Poukey J W and Rostoker N 1971 *Plasma Phys.* **13** 897
Rosinskii S E, Rukhadze A A and Ruhlin V G 1971 *Tech. Phys. Lett.* **14** 53
[22] Ignatov A M and Rukhadze A A 1977 *Bull. Lebedev Phys. Inst.* **11** 13
Peter W, Fael R J, Snell Ch and Jones M E 1985 *IEEE Transactions on Nuclear Science* **NS-32** 3506
[23] Ignatov A M and Tarakanov V P 1994 *Phys. Plasmas* **1** 741
[24] Dubinov A E, Kornilov I Y and Selemir V D 2002 *Usp. Fiz. Nauk.* **172** 1225
Belensov P E 2004 *Usp. Fiz. Nauk.* **174** 221

[25] Tarakanov V P 1992 *User's Manual for Code KARAT* (Springfield, VA: Berkley Research Associates)
[26] Kurilenkov Yu K, Skowronek M and Tarakanov V P 2006 *33rd Conf. on Plasma Physics and Controlled Fusion (Russia, Zvenigorod, Feb. 2006)*
Kurilenkov Yu K, Skowronek M and Tarakanov V P 2006 *Plasma Physics and Controlled Fusion* (Bristol: Institute of Physics Publishing) to be submitted
[27] Miley G H 2002 *US-Japan 5th Workshop on IECF (Wisconsin, Oct. 2002)*
Kulcinski G L *US-Japan 5th Workshop on IECF (Wisconsin, Oct. 2002)*
Hirsch R I 1967 *J. Appl. Phys.* **38** 4522
[28] Onishi M, Sato K H, Yamamoto Y and Yoshikwa K 1997 *Nucl. Fusion* **37** 611
[29] Kurilenkov Yu, Skowronek M and Konev Yu 2005 *Proc. 15th Int. Conf. on MHD Energy Conversion and 6th Workshop on Magnetoplasma Aerodynamics for Aerospace Applications (Moscow, 24–27 May)* pp 174–80
[30] Naranjo B, Gimzewski J K and Putterman S 2005 *Nature* **434** 1115–7